

Phonon dispersion of the bcc phase of group-IV metals. II. bcc zirconium, a model case of dynamical precursors of martensitic transitions

A. Heiming

*Institut Laue-Langevin, 156X, F-38042 Grenoble CEDEX, France
and Institut für Festkörperphysik der Universität Wien, A-1090 Wien, Austria*

W. Petry

Institut Laue-Langevin, 156X, F-38042 Grenoble CEDEX, France

J. Trampenau

*Institut Laue-Langevin, 156X, F-38042 Grenoble CEDEX, France
and Institut für Metallforschung, Universität Münster, D-4400 Münster, Germany*

M. Alba

Institut Laue-Langevin, 156X, F-38042 Grenoble CEDEX, France

C. Herzig

Institut für Metallforschung, Universität Münster, D-4400 Münster, Germany

H. R. Schober

Institut für Festkörperforschung der KFA-Jülich, D-5170 Jülich, Germany

G. Vogl

Institut für Festkörperphysik der Universität Wien, A-1090 Wien, Austria

(Received 11 September 1990)

The phonon dispersion of the high-temperature bcc phase of Zr has been measured at several temperatures. The longitudinal $L_{\frac{2}{3}}(1,1,1)$ mode and the transverse $T_1\frac{1}{2}(1,1,0)$ mode with $[1\bar{1}0]$ polarization are of very low energy (i.e., of large amplitude) and overdamped. These phonons achieve the displacements necessary for two martensitic phase transitions. The $L_{\frac{2}{3}}(1,1,1)$ phonon displaces the lattice toward the high-pressure ω phase and the $T_1\frac{1}{2}(1,1,0)$ phonon shifts the bcc planes into the stacking sequence of the low-temperature hcp phase. These fluctuations are interpreted as *dynamical* precursors of the low-symmetry phases within the bcc phase. *Elastic* precursors or central peaks were not found in pure bcc Zr. Furthermore, it is shown that the bcc phase is stabilized mainly by the excess vibrational entropy due to the low-energy phonons.

I. INTRODUCTION

This work, which belongs to a series of papers reporting the phonon dispersion of the bcc, or β , phase of the three group-IV metals, discusses measurements on pure β -zirconium. The papers dealing with β -Ti (Refs. 1 and 2) and β -Hf (Ref. 3) are referred to as I and III, respectively. The dispersions of these metals are of particular interest for an understanding of the anomalous self-diffusion⁴⁻⁷ and an understanding of the dynamics of the phase transitions: The high-temperature bcc structure of Ti, Zr, and Hf transforms martensitically to the low-temperature hcp α phase and to the high-pressure hexagonal ω phase.⁸

Experimental studies of the reasons for the martensitic phase transitions (MT) in β -Zr are interesting, because many theoretical investigations refer explicitly to this element as a model system for low-frequency phonons acting as precursor for first-order phase transitions. Ye

*et al.*⁹ studied the stability of the high-temperature bcc phase by frozen-phonon calculations, taking into account anharmonicity to fourth order. Lindgård and Mouritsen^{10,11} considered a Landau free-energy expansion for Zr in terms of two fluctuating strains and construct a magnetic-analog model for martensitic phase transitions. Dmitriev *et al.*¹² generalized and extended this expansion to include the β -to- ω transition. Krumhansl and Gooding¹³ showed that small changes in some low-frequency phonon modes which do not necessarily need to completely soften drive the martensitic transition (MT). Molecular-dynamics simulations performed on Zr (Ref. 14) and frozen-phonon calculations⁹ revealed the importance of the vibrational and formation entropy in stabilizing the bcc structure at high temperature. All these investigations predict precursor effects in terms of low-frequency phonons distributed over a wide range of energy, whose frequencies decrease as the phase transition is approached. Furthermore, they indicate that, at the expense of decreasing phonon energies, elastic intensi-

ty or a central peak should develop at the same location in reciprocal space, due to the formation of local clusters of the new phase. This elastic intensity should drastically increase as the transition temperature T_0 is approached.

Although the phonon dispersion of pure bcc Zr has already been measured at 1150 °C by Stassis *et al.*^{15,16} no further details on anharmonicity effects, such as temperature-dependent or broadened phonon branches, are available. Here we report on a study of the temperature dependence of the phonon dispersion in β -Zr over the whole range of existence of the bcc phase (862 °C < T < 1852 °C). After a presentation of experimental details (Sec. II), it will be shown that phonons in β -Zr are indeed strongly anharmonic (Sec. III). Section IV reveals the nonexistence of elastic precursors of the MT's and in Sec. V the results of Born-von Kármán calculations and related quantities are presented. It is shown that the high-temperature bcc phase is stabilized mainly by the low-energy phonons.

II. EXPERIMENTAL DETAILS

High-purity iodine-grade Zr bars (three different lots supplied by Teledyne Wah Chang, Albany, USA) were used as starting materials for sample preparation. The chemical analysis on gaseous and metallic impurities given by the supplier showed no noticeable differences between the different lots. The results on lot No. 3 are (in wt. ppm): [Al] < 1, [B] 0.25, [C] < 30, [Cd] < 0.25, [Co] < 10, [Cr] < 50, [Cu] < 10, [Fe] 148, [H] 8, [Hf] 53, [Mn] < 25, [Mo] < 10, [N] < 5, [Nb] < 50, [Ni] < 35, [P] < 4, [Pb] < 25, [Si] 25, [Sn] < 10, [Ta] < 50, [Ti] < 25, [U] < 1, [V] < 25, and [W] < 25. The additional analysis of the oxygen and nitrogen content performed by the Bundesanstalt für Material Prüfung, Berlin, using the hot-extraction method yielded 31(5) and 4(1) wt.ppm, respectively.

To avoid contamination by gaseous impurities, rods 100 mm in length and 10 mm in diameter were machined out of the raw material without undergoing any melting process. These rods were used for single-crystal growth. To overcome the experimental problem related to the MT at $T_0 = 862$ °C, which destroys any bcc single crystal into different hcp grains upon cooling, a combined crystal-growth and measuring furnace^{17,18} designed for neutron-scattering experiments was used. One of the essential ideas of this furnace is the crucible-free growth of single crystals. Samples were fixed by a cooled screw made of Mo at the top and bottom of sample rods. Crystals were grown under high vacuum by zone melting *in situ* on the neutron spectrometer and were permanently kept above T_0 . This approach is different from the method used by Stassis *et al.*,^{15,16} in which bcc single crystals were obtained by frequent cycling of an original hcp single crystal through the β -to- α transition. During our growth process, the approximately 2-mm-high molten zone was observed through a stereographic microscope. The melt was moved upwards through the sample rod using a speed of ~ 30 mm/h, thereby growing a sin-

gle crystal of roughly 50 mm in length. After the end of the growth process, the temperature of the sample was maintained well above the transition temperature. This was achieved by switching on an alternating current passing through the sample and a slow increase of it, whereby the high-frequency power was gradually reduced. To minimize the adsorption of gaseous impurities, crystal rods were never used twice. Analysis on gaseous impurities of one typical Zr sample after five days of experiments at high temperatures yielded oxygen and nitrogen concentrations of 710(60) and 12(3) wt.ppm, respectively.

The single crystals so obtained were then orientated on the three-axis spectrometer. Rocking curves indicated a typical width of the (110) reflection of 0.25° which roughly corresponds to the spectrometer resolution.

All experiments were performed on the thermal-neutron three-axis spectrometer IN8 at the high-flux reactor of the Institut Max von Laue-Paul Langevin. The conditions were very similar to those used for the study of β -Ti described in I.² For the definition of the scattering plane in reciprocal-lattice units (r.l.u.), our own high-precision-measurement values of the lattice parameter,¹⁸ $a(T) = 3.574(3) + [3.37(27)] \times 10^{-5} T(\text{K})$ Å was used.

III. PHONON DISPERSION OF β -Zr AT VARIOUS TEMPERATURES

Some results of phonons in β -Zr, which are related to the β -to- α and β -to- ω transition, have been reported earlier in a short communication.¹⁹ These results have been included in the following analysis.

All phonons measured either in constant- $(\hbar\omega)$ or constant- q mode²⁰ are given in Tables I and II. The errors account for the statistical errors as calculated by fitting the spectra by Gaussian or damped-oscillator functions. Systematic errors, as they become evident when the same phonon is measured on different crystals or in different Brillouin zones but otherwise under similar conditions, are not included. Only at low q do the systematic errors exceed the statistical errors.

Figures 1 to 3 show the phonon dispersion of β -Zr measured at temperatures at 915 °C, 1210 °C, and 1610 °C. The dispersion of β -Zr resembles very much that of β -Ti. The general decrease of the frequencies in β -Zr in comparison to β -Ti follows the homology rule $\omega_{\text{Zr}}/\omega_{\text{Ti}} = (m_{\text{Ti}}/m_{\text{Zr}})^{1/2}(a_{\text{Ti}}/a_{\text{Zr}})$. Comparing to the phonon dispersion of group-V and -VI metals, several anomalies become evident. (1) The L $[\xi\xi\xi]$ phonon branch has an extreme dip at $\xi = \frac{2}{3}$. (2) For large ξ , the transverse $[\xi\xi 0]$ phonon branch (T_1) with $[1\bar{1}0]$ polarization is of unusual low energy. These two results have already been reported by Stassis *et al.*^{15,16}

Additionally the present measurements reveal that (3) the intensity of the L $\frac{2}{3}(1,1,1)$ phonon mode is distributed down to zero energy transfer, (4) the T_1 $[\xi\xi 0]$ phonon branch shows an anomalous temperature dependence and (5) the L $\frac{2}{3}(1,1,1)$ and the T_1 $\frac{1}{2}(1,1,0)$ phonons are connected via a band of low energy and strongly damped phonons along $[\xi\xi 2\xi]$.

TABLE I. Phonons in bcc Zr measured at various temperatures and fitted with a Gaussian line shape.

915 °C		L [$\xi\xi\xi$] 1210 °C		1610 °C	
ξ	$\hbar\omega$ (meV)	ξ	$\hbar\omega$ (meV)	ξ	$\hbar\omega$ (meV)
0.066(2)	6.0	0.037(6)	4.0	0.045(7)	6.0
0.089(2)	8.0	0.050(7)	5.0	0.083(4)	8.0
0.198(6)	17.0	0.065(2)	6.0	0.117(3)	11.0
0.300	19.8(2)	0.084(3)	8.0	0.162(7)	14.0
0.432(4)	17.0	0.093(3)	9.0	0.300	18.57(15)
0.485(3)	15.0	0.125(3)	12.0	0.454(3)	17.0
0.538(2)	12.0	0.159(4)	15.0	0.478(5)	15.0
0.564(3)	10.5	0.201(5)	17.0	0.544(6)	12.0
0.607(13)	9.0	0.300	19.3(3)	0.602(24)	9.0
0.629(2)	7.5	0.436(3)	17.0	0.627(9)	7.5
0.638(2)	6.0	0.475(3)	15.0	0.662(9)	7.5
0.643(1)	3.0	0.511(2)	13.5	0.639(2)	6.0
0.654(2)	0.0	0.533(4)	12.0	0.645(3)	3.0
0.727(5)	7.5	0.569(2)	10.5	0.654(2)	0.0
0.72(3)	9.0	0.608(5)	9.0	0.723(27)	9.
0.732(4)	10.5	0.592(6)	7.5	0.757(7)	12.0
0.756(3)	15.0	0.639(2)	6.0	0.804(7)	15.0
0.807(3)	15.0	0.644(2)	4.5	0.900	17.8(3)
0.925	19.2(2)	0.643(2)	3.0	1.000	18.9(3)
1.000	19.8(2)	0.648(2)	0.0		
		0.689(6)	7.5		
		0.726(5)	10.50		
		0.730(8)	9.0		
		0.753(7)	12.0		
		0.774(2)	13.5		
		0.827(3)	15.0		
		1.000	19.04(15)		

915 °C		T [$\xi\xi\xi$] 1210 °C		1610 °C	
ξ	$\hbar\omega$ (meV)	ξ	$\hbar\omega$ (meV)	ξ	$\hbar\omega$ (meV)
0.059(1)	2.0	0.056(1)	2.0	0.132(1)	4.0
0.131(1)	4.0	0.127(1)	4.0	0.194(2)	6.0
0.194(2)	6.0	0.195(2)	6.0	0.298(5)	9.0
0.305(6)	9.0	0.308(9)	9.0	0.397(7)	12.0
0.437(10)	12.0	0.402(9)	12.0	0.53(2)	15.0
0.54(20)	15.0	0.513(9)	15.0	0.53(1)	16.0
0.57(10)	16.0	0.60(3)	16.0	0.80	18.8(3)
0.80	18.7(5)	0.80	18.6(3)	0.90	17.4(1.2)
0.90	20.3(4)	0.90	19.3(7)		

T ₂ [$\xi\xi0$] 915 °C		1210 °C		L [00 ξ] 1150 °C	
ξ	$\hbar\omega$ (meV)	$\hbar\omega$ (meV)	ξ	$\hbar\omega$ (meV)	$\hbar\omega$ (meV)
0.10		1.67(10)	0.106(1)	5.0	0.22(3)
0.20	6.9(2)	6.9(2)	0.40(1)	14.0	0.304(2)
0.25	8.3(3)	8.3(3)	0.80	19.84(7)	0.53(7)
0.30	9.2(3)	9.1(3)			0.67(9)
0.276(6)	10.0				17.50

915 °C		L [$\xi\xi0$] 1210 °C		1150 °C	
ξ	$\hbar\omega$ (meV)	ξ	$\hbar\omega$ (meV)	ξ	$\hbar\omega$ (meV)
0.028(1)	2.0	0.029(1)	3.00	0.059(1)	4.0
0.058(1)	4.0	0.067(1)	4.50	0.105(1)	7.0
0.090(1)	6.0	0.098(2)	6.00	0.153(1)	10.0

TABLE I. (Continued).

915°C		L [$\xi\xi0$] 1210°C		1150°C	
ξ	$\hbar\omega$ (meV)	ξ	$\hbar\omega$ (meV)	ξ	$\hbar\omega$ (meV)
0.113(1)	7.5	0.114(1)	7.50	0.204(1)	13.0
0.134(1)	9.0	0.138(9)	9.00	0.245(1)	15.0
0.159(1)	10.5	0.187(1)	12.00	0.299(2)	17.0
0.185(1)	12.0	0.244(2)	15.0	0.40	18.3(3)
0.121(1)	13.5			0.50	18.9(4)
0.242(2)	15.0				
0.30	17.0(1)				
0.40	19.0(2)				
0.50	19.5(2)				

L		T ₂	
ξ	$\hbar\omega$ (meV)	ξ	$\hbar\omega$ (meV)
0.036(1)	5.0	0.096(1)	5.0
0.071(1)	9.0	0.171(1)	9.0
0.121(1)	14.0	0.230(2)	12.0
0.155(2)	17.0	0.291(3)	15.0
0.200	18.94(15)	0.337(4)	17.0
0.250	19.1(2)	0.400	17.5(2)
0.330	17.0(3)		
0.38(8)	17.0		
0.450	15.0(3)		
0.500	14.0(5)		

TABLE II. Phonons in bcc Zr measured at various temperatures and fitted with a damped oscillator including convolution with the instrumental resolution.

ξ	895°C		960°C		T ₁ [110] 1150°C		1295°C		1610°C	
	$\hbar\omega$ (meV)	Γ (meV)	$\hbar\omega$ (meV)	Γ (meV)	$\hbar\omega$ (meV)	Γ (meV)	$\hbar\omega$ (meV)	Γ (meV)	$\hbar\omega$ (meV)	Γ (meV)
0.10	1.58(8)	0 ^a	1.67(10)	0.2 ^a	1.77(10)	0.1 ^a	1.80(10)	0 ^a	2.75(12)	0 ^a
0.15					2.64(10)	0 ^a				
0.20	3.07(12)	1.0(1)	3.09(10)	1.0(1)	3.37(8)	1.12(3)	3.42(10)	1.10(3)	4.94(12)	3.7(4)
0.25			3.72(10)	1.53(6)	3.96(10)	1.61(6)	4.07(10)	1.54(4)		
0.30	4.10(12)	2.0(1)	4.16(10)	2.22(9)	4.51(12)	2.32(8)	4.61(12)	2.20(5)	5.72(21)	3.3(7)
0.35	4.42(13)	2.6(2)			4.95(11)	2.9(1)	5.10(11)	3.02(1)		
0.40	4.76(10)	3.3(2)	4.62(10)	3.4(2)	5.10(10)	3.3(2)	5.37(11)	3.4(2)	6.63(20)	3.1(5)
0.45	4.45(13)	3.2(3)	5.01(12)	3.8(3)	5.42(10)	4.2(2)	5.80(12)	4.0(2)	6.88(20)	3.7(6)
0.50	4.48(11)	3.8(3)	4.90(11)	3.9(3)	5.42(10)	4.3(2)	5.77(12)	4.1(2)	6.91(20)	4.2(4)

T ₁ [$\xi\xi2\xi$] 960°C		
ξ	$\hbar\omega$ (meV)	Γ (meV)
0.05	1.99(8)	0 ^a
0.10	3.40(15)	0.1 ^a
0.15	5.10(15)	0 ^a
0.20	6.13(15)	3.6(3)
0.25	6.68(12)	5.9(3)
0.30	6.59(14)	6.7(4)
0.33	7.50(50)	9.9(5)
0.40	6.58(12)	6.4(3)
0.45	5.81(11)	5.5(3)
0.50	4.95(12)	4.6(3)

^aAt small q focussing effects become dominant and the intensity is no longer distributed symmetrically in energy loss and gain. Gaussian fits were used and Γ indicates the broadening with respect to the measured resolution.

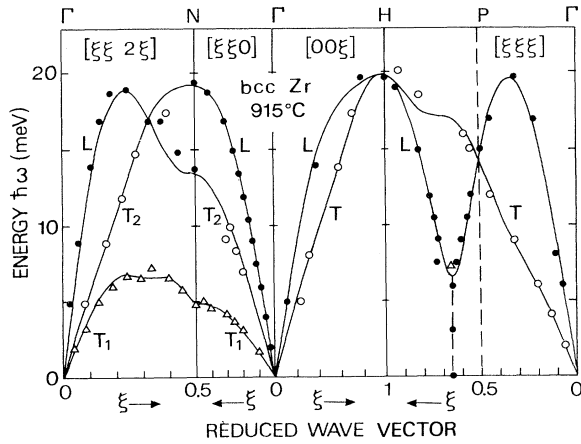


FIG. 1. Phonon dispersion in bcc Zr measured at 915°C (the $[00\xi]$ direction has been measured at 1150°C, the T_1 $[\xi\xi 2\xi]$ and T_1 $[\xi\xi 2\xi]$ phonon branch at 960°C). The solid line shows the results of a BvK fit using force constants up to the fifth nearest-neighbor shell (also in Figs. 2 and 3).

A. Longitudinal phonons around $q = \frac{2}{3}(1, 1, 1)$

As discussed in I,² the $L \frac{2}{3}(1, 1, 1)$ phonon displaces two neighboring $(1, 1, 1)$ planes towards or apart from each other whereas every third plane stays at rest. If the two moving planes collapse, the ω phase is obtained. Due to its close relation to the ω phase, we call $q = \frac{2}{3}(1, 1, 1)$, the ω point.

Constant-energy scans at 1210°C around the ω point in the $\tau = (2, 2, 2)$ Brillouin zone (BZ) are shown in Fig. 4(a) and illustrate the meaning of the dashed line in Figs. 1 to 3. At high energy transfer, two well-separated phonons are found which approach each other at lower energy. A separation between the two phonons is no longer possible below approximately $\hbar\omega \sim 7$ meV. The width in q (fwhm)

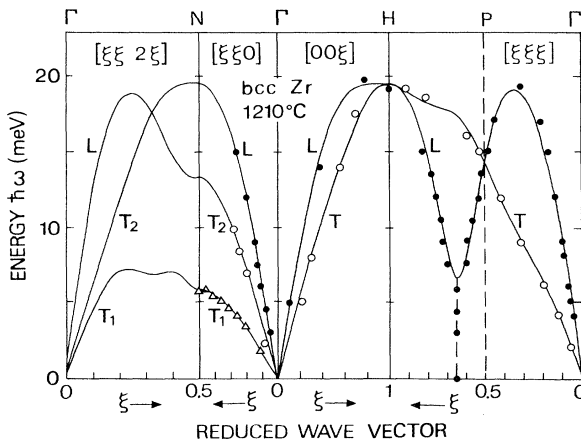


FIG. 2. Phonon dispersion in bcc Zr measured at 1210°C (the $[00\xi]$ direction has been measured at 1150°C, the T_1 $[\xi\xi 2\xi]$ branch at 1290°C).

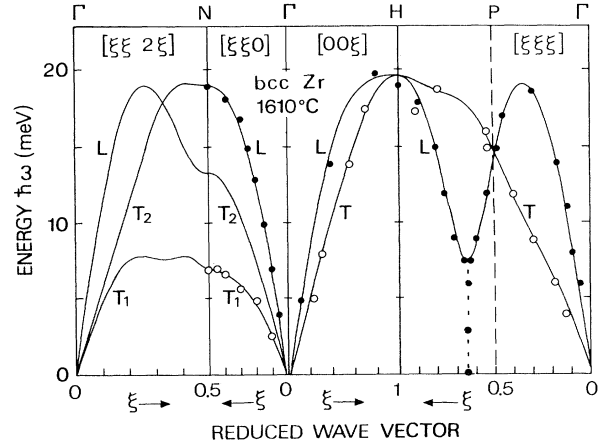


FIG. 3. Phonon dispersion in bcc Zr measured at 1610°C (the data along the $[00\xi]$ direction stem from measurements at 1150°C).

approaches 0.1 r.l.u. This width is beyond the instrumental resolution of 0.01 r.l.u. at zero energy transfer. The *coherent* intensity reaches down to zero energy transfer with almost equal intensities between $\hbar\omega = 6$ and 0 meV. In the present case being coherent means that the neutron spectra shown in Fig. 4(a) have been corrected for the purely incoherent background (see I). As shown in Fig. 4(a) the intensity at $\hbar\omega = 0$ does not exceed the intensity of the neighboring inelastic one. Therefore, in analogy to the arguments presented in I,² it is concluded that the intensity at zero energy transfer is inelastic in origin.

This distribution of inelastic scattered intensity extending from $\hbar\omega = 0$ to approximately 15 meV is illustrated by constant- q scans along the top of the phonon groups at $Q = 1.35(1, 1, 1)$. Figure 4(b) shows such spectra measured at three different temperatures which represent the whole range of existence of the bcc phase in Zr. Notice that in Fig. 4(b) the incoherent and background scattering intensity has not been subtracted and therefore appears as a cusp around $\hbar\omega = 0$.

As shown in I,² a phonon of the energy $\hbar\omega$ having a finite lifetime due to a damping Γ can be described by a damped oscillator.²¹ In this case, the phonon width $\Gamma = 2\hbar/\tau$ has the meaning of an inverse relaxation time. Overdamping occurs when $\Gamma > \hbar\omega_0$, with ω_0 being the frequency of the unperturbed oscillator.

The spectra shown in Fig. 4(b) were fitted by a damped oscillator, including the convolution with the instrumental resolution and an extra elastic line of Gaussian shape to describe the elastic incoherent scattering. As it can already be judged from the spectra in Fig. 4(b), the $L \frac{2}{3}(1, 1, 1)$ phonon in β -Zr does nearly not change its shape with temperature. With $\Gamma \sim 10(1)$ and $\hbar\omega_0 \sim 8(1)$ meV, this phonon is overdamped and a phonon lifetime of $\tau = 1.4 \times 10^{-13}$ s is calculated. It turns out that the characteristic feature of anharmonicity (i.e., damping) is less pronounced in β -Zr than in β -Ti [compare Fig. 4(b) of I²]. This behavior is expected for a classical damped

oscillator, because for such a system the damping is proportional to the inverse mass.

In I,² we have already argued that the $L_{\frac{2}{3}}(1,1,1)$ phonon has the only wave vector which moves [111] chains against each other without altering the nearest-neighbor distance within a given [111] chain (see Fig. 5 in I²). The corresponding phonon frequency is due to weak restoring forces between the chains. All other modes with $[\xi\xi\xi]$ propagation will change the nearest-neighbor distance of the atoms along the chains (for which stronger restoring forces are expected) and this gives rise to higher phonon energies. This purely geometrical argument is valid for all bcc metals and in order to differentiate between various elements the specific electronic configurations have to be considered.

The attractive point for the experimentalist is that band-structure calculations exist for the specific case of bcc Zr. *Ab initio* calculations by Ho *et al.*^{22,23} show that

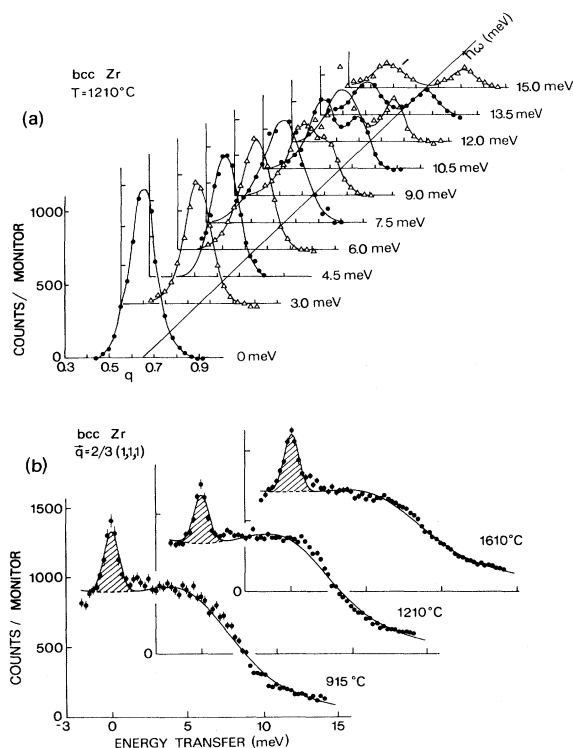


FIG. 4. (a) Constant $\hbar\omega$ scans in bcc Zr with $q \parallel [\xi\xi\xi]$ for different energy transfers. For $\hbar\omega=0$, the measured incoherent scattering has been subtracted. Fits with one or two lines of Gaussian shape of nearly constant width are shown. In this and all following figures the counts have been normalized to the incoming flux (monitor rate = 1000). (b) Uncorrected constant- q scans in bcc Zr at $Q=1.35(1,1,1)$. The shaded area indicates the elastic incoherent scattering. Fits with a damped oscillator including the convolution with the instrumental resolution are shown. The PG(002) monochromator, 50'-20'-20'-20' collimation, a PG(002) analyzer and constant $k_F=2.662 \text{ \AA}^{-1}$ have been used.

in bcc Zr the valence-charge density is concentrated in d bonds which run in chains along [111] direction with very little interaction between neighboring chains, i.e., the valence charge is highly localized along these [111] chains. As mentioned above, the $L_{\frac{2}{3}}(1,1,1)$ phonon is the only one which leaves the [111] chains undisturbed, i.e., does not compress or stretch the highly localized d bonds. The validity of these considerations is underlined by results from similar calculations for bcc Mo.^{22,23} Here, the d bonds entangle the [111] chains and oppose the shearing motion between neighboring [111] chains. Therefore the $L_{\frac{2}{3}}(1,1,1)$ phonon is not expected to have a particularly low frequency, perfectly agreeing with the experimentally determined phonon dispersion of Mo. Ho *et al.* used the so-called frozen-phonon technique and calculated the change in total energy of the crystals as the atoms are moved according to the displacement pattern of the $L_{\frac{2}{3}}(1,1,1)$ phonon in bcc Zr. For small displacements, they obtain the phonon frequency for bcc Zr within a harmonic approximation at 0 K. For large displacements, these calculations reveal the instability of the bcc structure towards the hexagonal ω structure at 0 K.

The pronounced dip of the $L_{\frac{2}{3}}[\xi\xi\xi]$ phonon branch at $\xi=\frac{2}{3}$ is also obtained by molecular-dynamics simulations of Willaime and Massobrio.¹⁴ These calculations are based on a simple tight-binding potential which reproduces the phonon dispersion of hcp α -Zr.

Table III compares the theoretical estimates of both groups with the measured phonon frequencies in bcc Zr. In view of the required precision for such total energy calculations, the agreement is surprisingly good.

Figure 4(b) shows that the ω phonon does not change significantly (beyond intensity changes due to the Debye-Waller factor) over the whole temperature range of the bcc phase at ambient pressure. This demonstrates that the ω phonon manifest an intrinsic weakness of the bcc structure of Zr for displacements towards the ω phase. The anharmonicity of these fluctuations is underlined by its strong damping in time. Independently from our experimental observations, theoretical calculations show the importance of anharmonicity to stabilize the bcc structure at high temperatures.

B. Transverse phonons with $[\xi\xi 0]$ propagation and $[1\bar{1}0]$ polarization

As discussed in I,² the β -to- α transformation can be achieved by the superposition of two phonons. The zone-boundary transverse phonon $T_1 \frac{1}{2}(1,1,0)$ at the N point with a displacement by $a\sqrt{2}/12$ of neighboring (110) planes in opposite $[1\bar{1}0]$ directions produces the hcp stacking sequence. Two equivalent long-wavelength shears—for instance, $(1\bar{1}2)[\bar{1}11]$ and $(\bar{1}12)[1\bar{1}1]$ —squeeze the bcc octahedron into a regular hcp one, thereby changing the angle from 109.5° to 120° .

Figure 5 shows phonon groups of the $T_1[\xi\xi 0]$ branch in β -Zr measured in constant- q mode. Evidently the phonon groups are very broad, the broadening increases with increasing ξ . Similar to the ω phonon, the appropriate line shape is given by a damped oscillator. The $T_1[\xi\xi 0]$ phonon branch was measured at various temperatures. A

TABLE III. Comparison of measured and calculated phonon energies in meV for bcc Zr at selected points in reciprocal space.

	$L \frac{2}{3}(1,1,1)$	H	$N T_1$	$N T_2$	$N L$
This work	7.5(5)	19.8(3)	4.48(11)	14.0(5)	19.5(2)
Measurement temperature T (°C)	960	915	895	960	960
Harmonic calculations	7.9 ^a		unstable ^c	14.9 ^c	
	9.0 ^b	21.3 ^b	unstable ^b	15.0 ^b	23.3 ^b
Anharmonic calculations			4.1 ^d	16.1 ^d	21.1 ^d
			4.6 ^e		

^aFrozen phonon at 0 K, Ref. 22.

^bMolecular dynamics at 0 K, Ref. 14.

^cFrozen phonon at 0 K, Ref. 25.

^dFrozen phonon including anharmonicity at 1400 K, Ref. 9.

^eMolecular dynamics at 1188 K, Ref. 14.

summary of the results is shown in Fig. 6 and is given in Table II. The damping Γ is on the order of $\hbar\omega_0$ for all q . As a result, the channel with highest count rate no longer coincides with the center frequency.²⁴ In contrast to the $L \frac{2}{3}(1,1,1)$ phonon, this low-energy branch shows a strongly temperature-dependent center frequency. The phonon energy decreases with decreasing temperature but stays finite at T_0 . Its temperature dependence has been fitted by a straight line, yielding a slope of 0.34(4) meV/(100 K). The phonon width or damping Γ is the largest at the BZ boundary and is almost independent of temperature.

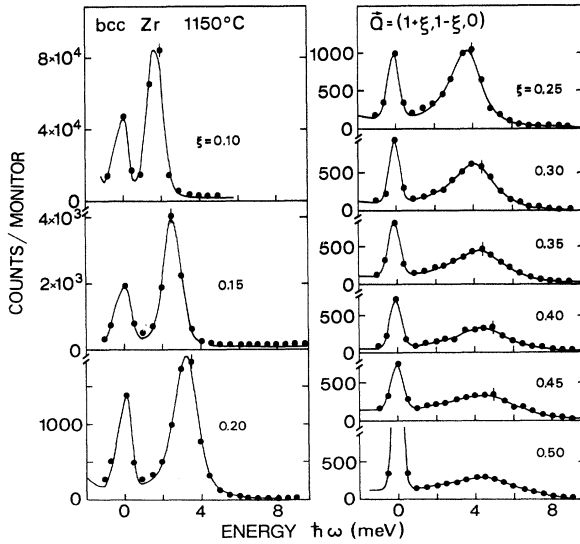


FIG. 5. Phonon spectra of the T_1 $[\xi\xi 0]$ branch in bcc Zr at 1150°C. The PG(002) monochromator 50'-20'-20'-20' collimation, a PG(002) analyzer and constant $k_F = 2.662 \text{ \AA}$ were used. The solid line shows fits with a damped oscillator, convoluted with the measured resolution. The peak at $\hbar\omega = 0$ stems from the incoherent elastic scattering. Note that also in this branch inelastic intensity can be found down to zero energy transfer.

Frozen-phonon calculations have also been performed for the longitudinal and transverse N -point phonon frequencies in bcc Zr.²⁵ Values are listed in Table III and are in agreement with our measurements. For the MT, the behavior of the T_1 N -point phonon is important because it shuffles neighboring (110) planes in a hcp stacking sequence. In the harmonic approximation and at 0 K, the bcc lattice is completely unstable against such displacements and only imaginary frequencies are found. However, by including anharmonic effects such as non-quadratic terms in the total-energy-versus-displacements plots and phonon-phonon coupling at elevated temperatures, a finite T_1 N -point phonon frequency of 4.1 meV at 1400 K is found.⁹ This frequency is lowest but nonzero at the phase transition and increases with increasing temperature. The calculations predict a slope of 0.8 meV/(100 K). Both the inverse temperature dependence and this slope for the T_1 N -point phonon were verified by us experimentally [Fig. 6(c)].

The anharmonic character of the stabilization of the bcc phase with respect to the close-packed hcp structure is confirmed by molecular-dynamic simulations for bcc Zr (Ref. 14) and a T_1 N -point phonon frequency of 4.6 meV is found above T_0 .

Recent thermodynamic approaches^{10,11,13} which use an expansion of the free energy in terms of the dynamical displacements have suggested that a small softening of the relevant low-energy phonon is sufficient to produce a lower minimum of the free energy to obtain the low-temperature phase. The order parameter in the expansion of the free energy is related to the average atomic displacements of the low-energy phonons which are associated with the transition mechanism. As argued by Dmitriev *et al.*,¹² the order parameter for the β -to- ω transition is a periodic function of the large amplitude of the ω phonon. In the case of the β -to- α transition, a coupling between the displacements of the T_1 N -point phonon and a long-wavelength shear mode has to be considered. This will be discussed in more detail in the next section.

Whereas a good theoretical understanding of the reason for the low energy of the T_1 N -point phonon is obtained, there exists no microscopic understanding for its

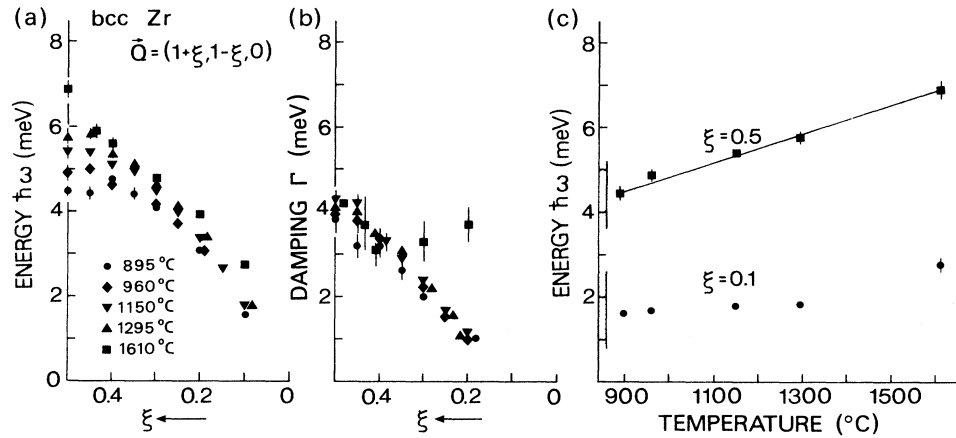


FIG. 6. Temperature dependence of the T_1 $[\xi\xi 0]$ phonon branch in bcc Zr. The results of fits with a damped oscillator with (a) the center energy $\hbar\omega_0$ and (b) the damping Γ are shown. (c) shows the temperature dependence of the T_1 $[\xi\xi 0]$ phonon branch at $\xi=0.1$ (initial slope) and at $\xi=0.5$. The temperature dependence of the T_1 $\frac{1}{2}(1,1,0)$ phonon has been fitted by a straight line with a slope of 0.34(4) meV/(100 K).

strong damping. The thermodynamic considerations^{10,11,13} propose a model for a continuous freezing of the large-amplitude phonons as the phase-transition temperature is approached. It is supposed that this freezing gets increasingly more important, as T_0 is approached. The experimental results do not confirm this picture: (1) The damping of the T_1 N -point phonon, which is observed over the whole temperature range of the bcc phase, is nearly independent of temperature. (2) The freezing should manifest itself in an elastic central peak, which is not observed (see also Sec. IV). Both items (1) and (2) point out rather that the large damping is intrinsic to the open structure of bcc Zr and the phase transition is not directly related to the damping.

C. Relation between the L $\frac{2}{3}(1,1,1)$ and the T_1 $\frac{1}{2}(1,1,0)$ phonon

In I^2 it was argued that the displacements of the L $\frac{2}{3}(1,1,1)$ phonon and of the T_1 N -point phonon are, respectively, identical to the transverse T_1 $\frac{1}{3}(1,1,2)$ and the T_1 $\frac{1}{2}(1,1,2)$ phonon. Furthermore, it could be shown that the displacements of the long-wavelength phonon of the T_1 $[\xi\xi 2\xi]$ phonon branch is very close to those of the $[11\bar{1}](112)$ shear. *This means that all phonons which achieve the displacements necessary for the two MT's lie in the same phonon branch with $[\xi\xi 2\xi]$ propagation and transverse polarization.* Because the L $\frac{2}{3}(1,1,1)$ and the T_1 $\frac{1}{2}(1,1,0)$ phonons are of low energy and are overdamped, it is concluded that they are connected via a band of low energy and strongly damped phonons along the $[\xi\xi 2\xi]$ direction.

Whereas we were not able to measure the T_1 $[\xi\xi 2\xi]$ phonon branch in β -Ti (see I^2), we could study this branch in β -Zr. Figure 7 shows phonon groups with $[\xi\xi 2\xi]$ propagation at 960°C. They are compared to

those of the T_1 $[\xi\xi 0]$ phonon branch. Obviously, for the whole $[\xi\xi 2\xi]$ branch, phonon intensities reach down to zero energy transfer. The elastic scattering at $\hbar\omega=0$, which originates from incoherent and background scattering, represents only a fraction of the intensity of the phonon scattering. Again, all spectra can well be described by a damped oscillator convoluted with the instrumental resolution. The deconvoluted phonon width or damping Γ is compiled in Table II.

The two phonons which are directly related to the phase transitions are connected by a valley of low energy and strongly damped phonons along $[\xi\xi 2\xi]$. These phonons are located on the surface of the BZ zone (see Fig. 10 of I^2). Contrary to long-wavelength shear modes, these large- q modes produce a maximum displacement of neighboring planes, i.e., they are best suited to shuffle bcc planes towards the stacking sequence of the low-symmetry phases. In the single-oscillator approximation, the amplitude u_0 of a vibration is given by

$$u_0 = \left[\frac{2k_B T}{m} \right]^{1/2} \frac{1}{\omega} . \quad (1)$$

The phonon energies $\hbar\omega$ are of the order of 4.5 meV, corresponding to displacements of about 0.7 Å. This is comparable to or even larger than the displacements needed for the actual phase transition. This suggests that this approximation is an oversimplification.

Because these phonons are overdamped, i.e., they have lifetimes on the order of one vibrational period, it is appropriate to speak of dynamical fluctuations. In real space, these large-amplitude fluctuations correspond to a continuous set of displacements which range from (110) planes shuffled into the hcp stacking sequence to (111) planes shuffled into the ω stacking sequence. Out of this bath of fluctuations only the displacements corresponding to the L $\frac{2}{3}(1,1,1)$ or to the T_1 $\frac{1}{2}(1,1,0)$ phonon—the

latter one coupled to the $\{112\}\langle 11\bar{1}\rangle$ long-wavelength shear—lock in at the transition.

IV. DEFECT-DRIVEN CONDENSATION OF LOW-ENERGY AND OVERDAMPED MODES

In view of the picture presented above of a locking in of large-amplitude fluctuations at the phase transitions, it is interesting to look for elastic precursors or central-peak phenomena which would precede the phase transition. Thermodynamic calculations^{10,11,13} discuss precursor effects in terms of local fluctuations into the low-symmetry phase. These metastable domains or embryos should have relatively long lifetime and therefore should appear in a neutron-scattering experiment with limited energy resolution as “elastic intensity.”

Neutron-scattering experiments on metal alloys²⁶ have revealed such elastic precursors with drastically increasing intensities as the MT is approached. Their location in q space is determined by the wave vector, related to the displacements necessary to effect the phase transition.

Careful corrections for contributions due to elastic incoherent scattering and to overdamped phonons enable us to investigate whether “truly” elastic scattering appears. The final result is that, in *pure* bcc Zr, there is no additional diffuse elastic scattering around the ω or N point, nor at temperatures close to T_0 .

This marked difference in the behavior of our pure samples with respect to alloys provokes the following question: Is the central peak a phenomenon generic for a martensitic phase transition? Or, turning the question around, to which extent is the condensation of a soft phonon into a central peak driven by point defects? In order to answer these questions, we alloyed bcc Zr with gaseous as well as metallic impurities, such as O, Nb, or Co, and performed extensive phonon measurements similar to those on the pure bcc Zr crystals.

First, pure bcc Zr crystals have been exposed to a constant air leak. This contamination of the samples with oxygen and nitrogen manifested itself in some puzzling observations. (1) As the temperature was lowered towards the bcc- to hcp-phase transition T_0 , the intensity of the bcc Bragg reflexions *decreased*, in contradiction to a Debye-Waller-factor dependence. (2) High-resolution scans around the (110) Bragg peak showed that this reflection was split, i.e., an additional peak at $Q=0.98(1,1,0)$ was observed [see Fig. 8(a)]. The intensity of this satellite increased exponentially with decreasing temperature. (3) Another, extremely temperature-dependent reflection appeared close to the ω point at $Q=1.28(1,1,1)$ [Fig. 8(b)]. This reflection had already been found during an earlier neutron-scattering investigation on bcc Zr (Ref. 15) and a possible relation to the high contamination of O in the samples (1.3 and 0.29

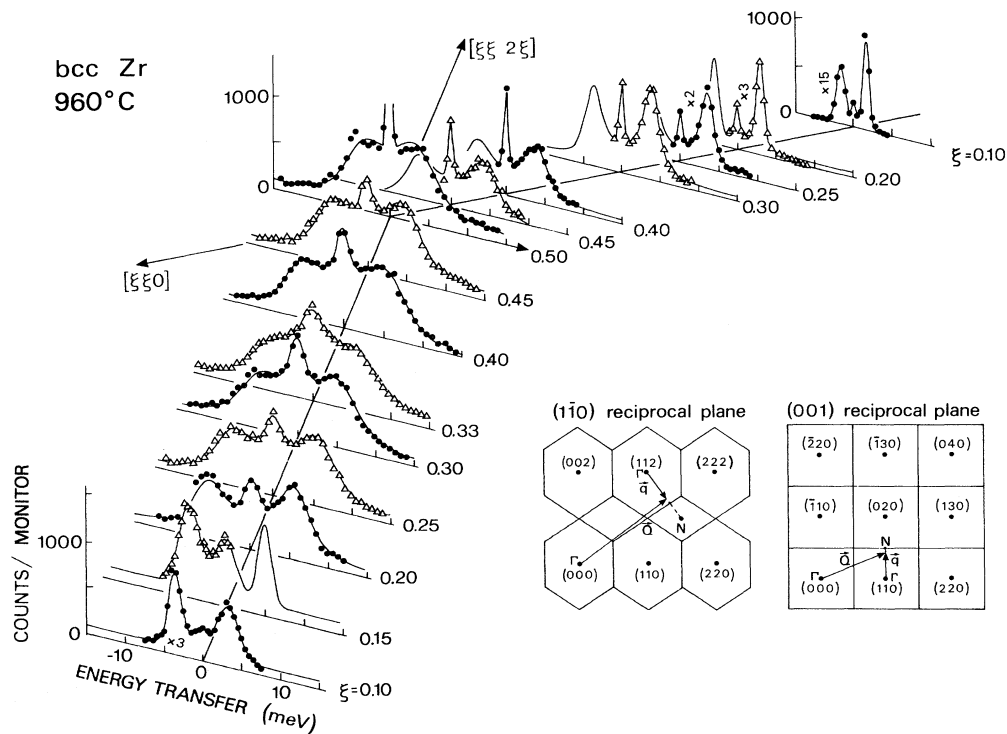


FIG. 7. Spectra of the T_1 $[\xi\xi 2\xi]$ phonon branch and of the T_1 $[\xi\xi 0]$ phonon branch in bcc Zr measured in the $(1\bar{1}0)$ and (001) plane, respectively. For the T_1 $[\xi\xi 2\xi]$ phonon branch, a Cu(111) monochromator, $50^\circ\text{-}40^\circ\text{-}40^\circ\text{-}40^\circ$ collimation and $k_F=4.1 \text{ \AA}^{-1}$ was used. The conditions for the T_1 $[\xi\xi 0]$ phonon branch are identical to those shown in Fig. 5. The elastic peak at $\xi=0.5$ is due to $\lambda/2$ scattering at $Q=(3,3,2)$.

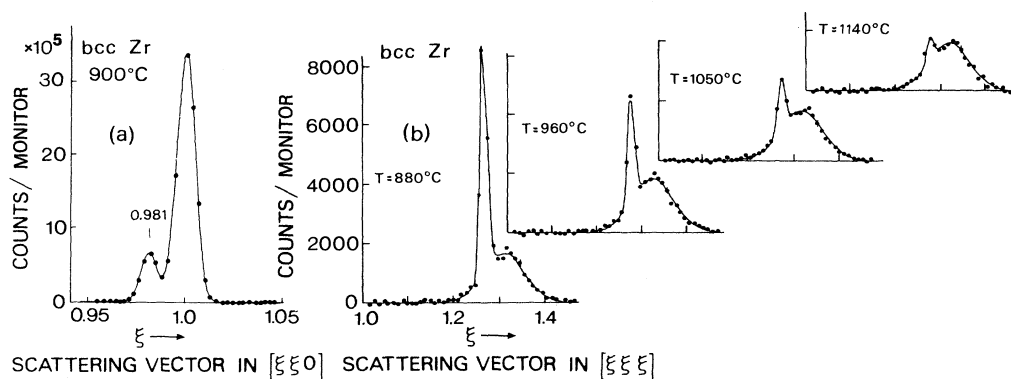


FIG. 8. (a) The split (110) bcc Bragg reflection in bcc Zr loaded with 0.46(2) wt.% oxygen. (b) Results of elastic measurements around the ω point at different temperatures for a sample loaded with 0.37(1) wt.% O. The narrow peaks are hcp Bragg peaks.

wt.% O) had been proposed. Its real origin, however, had never been unambiguously resolved. Since then, this peak has been interpreted as a possible precursor fluctuation of the ω phase.¹⁰

Analysis on gaseous impurities after our experiment revealed the absorption of several wt.% of oxygen in Zr. According to the Zr-O (Ref. 27) phase diagram, large amounts of oxygen can be dissolved in Zr. This leads to a temperature-dependent coexistence range of hcp and bcc at temperatures above T_0 . For instance, for Zr containing 0.5 wt.% O the hcp phase coexists with the bcc phase up to 250°C above the nominal transition temperature $T_0=862^\circ\text{C}$ for a pure sample. The Zr-N system has a similar phase diagram. Therefore, we explain the observations (1) to (3) by the coexistence of α and β phases due to alloying with O or N. A calculation of the reciprocal-lattice points of the hcp lattice in the bcc coordinate system according to the crystallographic relation of the β -to- α transition (Burgers's relation) demonstrates that this explanation is correct.^{18,19} A final verification of our ex-

planation was the prediction of new hcp reflections, which were always found exactly at the calculated positions. The width of these hcp Bragg peaks is comparable to the bcc Bragg peaks and given by the instrumental resolution, i.e., the hcp grain size is relatively large.

In a second step, pure bcc Zr was exposed to a small oxygen leak at a constant temperature of 1210°C. At this temperature, roughly 0.5 wt.% O can be dissolved without entering into the two-phase region.²⁷ Figure 9 shows results of measurements of the elastic diffuse scattering at the ω point after 14, 26, and 134 h of exposure to this leak. For comparison, inelastic scans at $\hbar\omega=3$ and 6 meV have also been performed. Due to the high temperature, the hcp peak shown in Fig. 8(b) is not visible. In the first measurement, after 14 h the elastic intensity is identical to the inelastic one. However, with increasing exposure time to oxygen, a clear increase of the diffuse scattering at $\hbar\omega=0$ is observed whereas the intensity at $\hbar\omega\neq 0$ remains unchanged. This broad diffuse intensity (fwhm=0.1 r.l.u.) changes only smoothly with

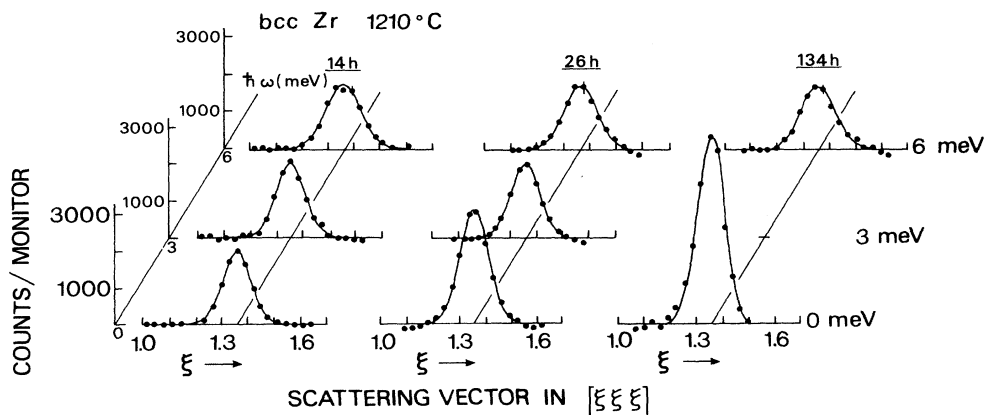


FIG. 9. Results of measurements around $Q=\frac{4}{3}(1,1,1)$ in bcc Zr for various energy transfers at different times during loading with oxygen.

temperature (on the order of a factor-of-2 change within the bcc temperature range). Thus a *true* elastic diffuse scattering intensity is found around the ω point.

In a further step, we alloyed metallic impurities such as Co or Nb to bcc Zr (Ref. 18). Nb is almost completely miscible with bcc Zr whereas Co does not fit into the bcc Zr lattice and therefore only a few at.% of Co can be dissolved. Measurements similar to those shown in Fig. 9 were performed. In both alloys, additional true elastic scattering near the ω point was found. Similar to results from the experiment in which we alloyed O to bcc Zr, this diffuse intensity does not alter significantly with temperature.

Consequently, two effects occur upon alloying.

(i) Interstitial impurities, such as oxygen and nitrogen, cause the coherent coexistence of the α and β phase above the nominal T_0 for a pure sample.

(ii) Substitutional and interstitial impurities cause static displacements, giving rise to elastic scattering. This diffuse elastic scattering is found in reciprocal space, where low-frequency phonons are also observed. With regard to the phase transitions, we emphasize that this elastic diffuse intensity is almost independent of temperature over the whole temperature range of the bcc phase. It should be considered as an intrinsic bcc property due to the interaction with defects rather than due to a continuous freezing of the phonon since the latter would gain in importance when approaching the transition. This view of the diffuse intensity being due to static displacements is strongly supported by the fact that we were not able to measure any quasielastic broadening, in energy, within the experimental resolution of 0.7 meV. This is in agreement with previous experiments on $Zr_{80}Nb_{20}$ alloys²⁸ in which measurements were performed with a resolution of 1 μ eV. In the measurements, a broadening of the elastic diffuse scattering at the ω point could not be detected either.

V. BORN-VON KÁRMÁN FITS AND RELATED PROPERTIES

A. Born-von Kármán fits

The measured phonon energies were fitted with a Born-von Kármán (BvK) model for the purpose of parametrization of the phonon dispersion. Within this phenomenological approach each atom vibrates harmonically around its equilibrium position and the interaction between neighboring atoms is described by force constants ϕ_{ij}^m . Anharmonic effects causing temperature shifts of the phonon energies are taken into account within the so-called quasiharmonic approach. The phonon dispersion, measured at three temperatures within the bcc phase, has been fitted with three different sets of ϕ_{ij}^m . Consistent with our fitting procedure used for Ti (paper I)² and Hf (paper III),³ forces up to the fifth-neighbor shell (13 parameters) were used. These fits are shown as the solid line in Figs. 1–3 and the ϕ_{ij}^m are listed in Table IV. This quasiharmonic BvK approach does not account for anharmonicity effects which cause a strong damping of the low-energy phonons.

TABLE IV. Interatomic force constants Φ_{ij}^m in bcc Zr. Force constants Φ_{ij}^m in dyn/cm obtained from Born-von Kármán fits to the dispersion curves in β -Zr at various temperatures.

	Zr 915°C	Zr 1210°C	Zr 1610°C
1 _{xx}	7351.7	7798.4	8140.2
1 _{xy}	8565.5	8341.7	7993.8
2 _{yy}	4967.6	4960.5	4564.7
2 _{yy}	−1952.8	−2170.2	−1898.2
3 _{xx}	615.3	838.6	634.1
3 _{zz}	−2083.0	−1410.0	−1582.6
3 _{xy}	1524.0	866.9	473.8
4 _{xx}	425.6	45.5	154.2
4 _{yy}	446.6	204.4	86.7
4 _{yz}	−1114.5	−995.4	−1064.7
4 _{xy}	−91.1	−134.9	79.7
5 _{xx}	−124.0	172.1	288.1
5 _{xy}	460.6	703.0	271.9

B. The phonon density of states

By following a procedure similar to that described in I,² the force constants ϕ_{ij}^m were used to calculate the normalized phonon density of states $Z(\omega)$. Results for the three temperatures are shown in Fig. 10. The first singularity corresponds to the low-lying and flat dispersion of the T_1 [$\xi\xi 0$] phonon branch. Its temperature dependence is clearly visible in $Z(\omega)$. The second singularity originates from the low-energy T_1 [$\xi\xi 2\xi$] phonon branch. At 1610°C, this branch and the T_1 [$\xi\xi 0$] phonon branch have nearly the same energy; therefore only one peak around $\hbar\omega = 7$ meV is observed. The local maxima around $\hbar\omega = 13$ meV are due to the BZ boundary phonons of the T_2 [$\xi\xi 0$] phonon branch. The split of the high-energy peak at $T = 915^\circ\text{C}$ must not be taken too seriously, because the experimental uncertainty in determining the high energy of H - and N -point phonons is too large.

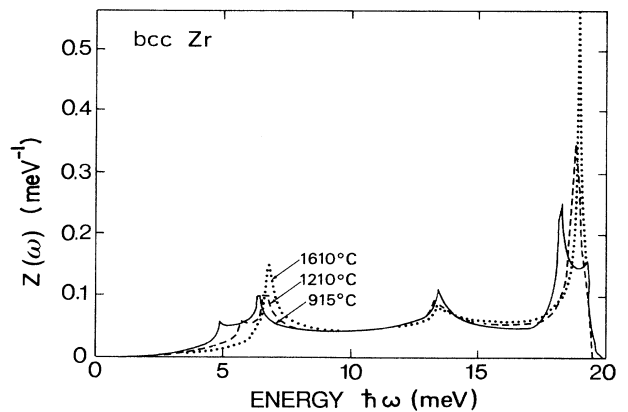


FIG. 10. Phonon density of states in bcc Zr at different temperatures.

C. The Debye temperature

From the phonon density of states the mean-square displacement $\langle u_i^2 \rangle$ of an atom can be calculated. This can be used to determine the Debye-Waller factor or the Debye temperature Θ_D . By means of Eq. (4) of I,² the temperature dependence of $\langle u_i^2 \rangle$ has been calculated and the result is shown in Fig. 11, where for the calculations $Z(\omega)$ has been taken from the measurement at 915°C (broken line). This harmonic temperature dependence of $\langle u_i^2 \rangle$ is compared to the results of calculations using $Z(\omega)$ directly from the measurements at the three different temperatures (quasiharmonic temperature dependence, solid line). Due to the unusual frequency increase for increasing temperature of the low-energy modes, a net stiffening of the lattice is observed. Therefore, the increase of $\langle u_i^2 \rangle$ for increasing temperature is less than would be expected for bcc Zr obeying an harmonic temperature behavior. According to Eq. (5) given in I,² $\Theta_D^2 \propto 1/\langle u_i^2 \rangle$, and the stiffening is also noticeable in an increase of Θ_D with increasing temperature.

D. Lattice specific heat and entropy

The lattice specific heat at constant pressure c_p can be calculated in the quasiharmonic approximation:

$$c_p = 3R \int_0^\infty d\omega Z(\omega) \frac{x^2}{\sinh^2 x} \left[1 - \frac{\partial \langle \ln \omega \rangle_\omega}{\partial \ln T} \right], \quad (2)$$

with $x = \hbar\omega/(2k_B T)$. In this expression, anharmonicity has been taken into account by including the temperature derivative of the phonon modes. Since only the frequencies of a small number of modes were measured at a few temperatures, an appropriate interpolation scheme is required for the analysis of the experimental data. An interpolation scheme similar to the one used by Stassis

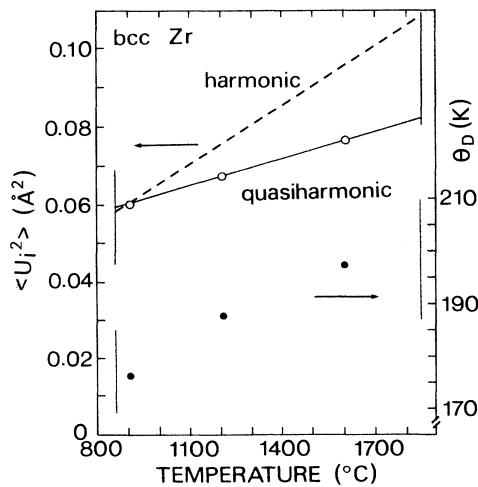


FIG. 11. Mean square displacement $\langle u_i^2 \rangle$ (\circ) and Debye temperature Θ_D (\bullet) calculated from $Z(\omega)$ at the corresponding temperature, (---) harmonic extrapolation of $\langle u_i^2 \rangle$ based on $Z(\omega)$ at 915°C; (—) guide to the eye.

*et al.*²⁹ has been adopted, with the following modification: Phonons below and above 10 meV have been interpolated separately because their change with temperature differs considerably. In the high-temperature limit $x \ll 1$, a lattice specific heat $c_p = 22.1 \times 10^7$ erg/(mol K) for bcc Zr has been calculated. With respect to a harmonic calculation [i.e., without the temperature derivative in Eq. (3)], this quasiharmonic value is reduced by roughly 10%.

The lattice or vibrational entropy has been calculated according to Eq. (6) of I² for the hcp (Refs. 29 and 30) and bcc phase of Zr. Results are given in Table V(a) and Fig. 12. The harmonic extrapolation based on the low-temperature measurements in the α or β phase is compared with quasiharmonic calculations based on phonon measurements at various temperatures. In the α phase, quasiharmonic entropies are larger than the harmonic entropies, whereas in the β phase, the opposite is the case. This anomalous “decrease” of entropies in the β phase is caused by the increase in frequency of the low-energy phonons with increasing temperature. We note that the behavior is anomalous because, with increasing temperature, metals usually become softer and their phonon frequencies decrease.

The gain in vibrational entropy at the transition ΔS_{vib} can be calculated by means of the quasiharmonic extrapolation of the entropies in the α and β phase at T_0 . $\Delta S_{\text{vib}} = 0.26 k_B/\text{atom}$ is found. For comparison, the total change in entropy is $\Delta S = 0.40 k_B/\text{atom}$,³¹ i.e., the electronic contribution can be estimated to $\Delta S_{\text{el}} = 0.14 k_B/\text{atom}$. This means that for Zr the lattice

TABLE V. (a) Lattice entropy of Zr calculated from the BvK parameters evaluated at the given temperature (column 3) and calculated (harmonically) from the BvK parameter at $T = 295$ K and $T = 1188$ K, respectively (column 4). (b) comparison of vibrational, electronic and total excess entropies at the β - to α -phase transition of Zr.

		(a)	
	T (K)	S_{vib} (k_B/atom)	S_{vib} (k_B/atom)
hcp	295	4.60 ^a	4.60
	773	7.74 ^a	7.44
	1007	8.62 ^a	8.23
bcc	1135	9.05 ^b	8.59
	1135	9.31 ^b	9.33
	1188	9.46	9.46
	1483	10.02	10.13
	1883	10.68	10.85
		(b)	
ΔS_{vib} (k_B/atom)	ΔS_{el} (k_B/atom)	ΔS_{total} (k_B/atom)	
0.26 ^c	0.185 ^d	0.40 ^f	
0.14 ^e			

^aReferences 29 and 30.

^bExtrapolated to T_0 .

^cThis work.

^dReferences 9 and 32.

^eReference 14.

^fReference 31.

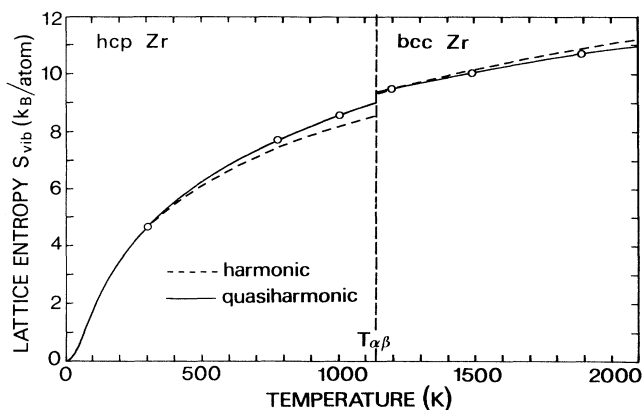


FIG. 12. Lattice vibrational entropy S_{vib} (\circ) calculated from $Z(\omega)$ at the corresponding temperature. The hcp values stem from measurements of Stassis *et al.* (Refs. 28 and 29) (---) harmonic extrapolation of S_{vib} based on $Z(\omega)$ at 25°C and 915°C; (—) second-order polynomial fit.

vibrational entropy accounts for $\sim 65\%$ of the excess entropy at the β -to- α transition. This is similar to our results for Ti, where 70% of the excess entropy are of vibrational origin (see I²).

These experimental findings may be compared with recent direct calculations of the electronic and vibrational part of the excess entropies of Zr. First-principles computations of the electronic density of states performed by Harmon and co-workers^{9,32} yield $\Delta S_{\text{el}} = 0.185 k_B/\text{atom}$, which compares well with our estimate. Furthermore, these calculations emphasize the important role of the low-energy T_1 N -point phonon and the ω phonon. Molecular-dynamics calculations of Willaime and Massobrio¹⁴ allow a direct computation of $\Delta S_{\text{vib}} = 0.143 k_B/\text{atom}$. This value is only half of our experimental value and therefore overestimates the electronic part. A summary of the different results is presented in Table V(b).

As shown above, the stability of the high-temperature phase is mainly due to the excess entropy of the low-energy phonons. It is interesting to note that in 1947 Zener³³ already proposed that the excess entropy needed to stabilize the bcc phase in group-IV metals originates from soft acoustic shear modes, i.e., *long-wavelength* modes. Later on, Friedel³⁴ suggested that the low-energy phonons which stabilize the bcc lattice are not shear modes but *short-wavelength phonons*. Qualitatively he argued that these short-wavelength phonons should be of lower frequency in the bcc structure than in the close-packed low-temperature structure. Contrary to Zener, we have shown that the modes stabilizing the bcc lattice are mainly found on the Brillouin-zone surface, i.e., they are of short wavelength and we thereby confirm the qualitative picture of Friedel.

This immediately provokes the question, “Why do group-V and VI metals which show no low-energy modes have bcc as their only structures.” As shown by the *ab initio* calculations of Ho *et al.*,^{22,23} these metals are stabi-

TABLE VI. Elastic constants for bcc Zr at different temperatures in 10^{12} dyn/cm², calculated from the force constants ϕ_{ij}^m .

T (°C)	C_{11}	C_{12}	C_{44}	$C' = \frac{1}{2}(C_{11} - C_{12})$	C_-
915	1.04	0.93	0.38	0.06	0.14
1210	0.97	0.82	0.40	0.08	0.16
1610	1.00	0.70	0.35	0.15	0.21

lized to bcc by d -electron bonding. Within the group-III to -VI transition metals, this electronic stabilization of bcc increases with increasing d -electron density. This is in agreement with the observation that in group-III metals the bcc phase has its narrowest range of existence. Group-I and -II metals show in their bcc phase low-energy phonon branches similar to those presented here and—with the exception of K and Rb—exhibit a transition to a close-packed structure either under pressure or temperature changes. The excess entropy at the transition is much smaller compared with those of group-IV metals³¹ and is presumably dominated by its vibrational part.³⁵

E. Elastic constants

Conventional sound-velocity measurements of the elastic constants in bcc Zr are not available. Therefore we calculated the elastic constants from the force constants ϕ_{ij}^m , according to a formula derived by Squires.³⁶ The results are summarized in Table VI which includes the elastic constant C_- which is obtained from the initial slope of the T_1 $[\xi \xi 2\xi]$ phonon branch. Using the values of C_{11} , C_{12} , and C_{44} a polarization vector $(1, 1 - 1.29)$ of the T_1 $[\xi \xi 2\xi]$ phonon branch as $\xi \rightarrow 0$ has been determined (see I²). Similar to results for β -Ti, the long-wavelength shear of the T_1 $[\xi \xi 2\xi]$ phonon branch in β -Zr corresponds roughly to the $[11\bar{1}]$ (112) shear needed for the β -to- α transition. C' and C_- exhibit an inverse temperature dependence, whereas C_{11} and C_{44} stay almost constant over the whole temperature range of the bcc phase. With respect to elastic constants, bcc Zr is a very anisotropic medium. According to the first-order character of MT's, C' stays finite at T_0 .

VI. CONCLUSIONS

The phonon dispersion of β -Zr resembles closely that of β -Ti (paper I²). In particular, we show the following.

(1) The L $[\xi \xi \xi]$ phonon branch has a pronounced dip at $\xi = \frac{2}{3}$ (ω point). This mode is overdamped with shoulders reaching down to $\hbar\omega = 0$. Neither the softening nor the damping changes with temperature.

(2) The whole T_1 $[\xi \xi 0]$ phonon branch with $[1\bar{1}0]$ polarization is of low energy and is overdamped. Furthermore, these phonons decrease in energy with decreasing temperature towards the β -to- α transition. This behavior is anomalous, because, with decreasing temperature, metals usually become harder and their phonon energies increase. These effects are most pronounced at $\xi = \frac{1}{2}$ (N point), i.e., at the Brillouin-zone boundary.

(3) The whole T_1 [$\xi\xi2\xi$] phonon branch, containing both the ω point and the N -point phonon, is of low energy and overdamped. Both, the T_1 [$\xi\xi0$] and T_1 [$\xi\xi2\xi$] phonons form a valley of low-energy phonons in the four-dimensional \mathbf{q} and $\hbar\omega$ dispersion surface. These low-energy fluctuations are related to the tendency of group-IV metals to undergo phase transitions. Out of this bath of large-amplitude fluctuations, only displacements corresponding to a shuffling of bcc planes into the hcp or the ω structure lock in at the respective phase transition.

For studying relations between the phonon dispersion and phase transitions, β -Zr is a "more developed model case" than β -Ti because many theoretical first-principles studies have dealt with low-frequency phonons as precursors of martensitic phase transitions in Zr. The phonon-related quantities calculated in the quasiharmonic approximation confirm the picture of a stabilization of the bcc structure with respect to the low-temperature close-packed structure by the lattice *vibrational excess entropy*. The temperature dependence of this excess entropy is caused by the low-energy phonons located on the BZ boundary. As a dynamical precursor, the T_1 N -point phonon decreases in energy as the β -to- α transition is ap-

proached. Different from soft modes or second-order transitions, the real phase transition occurs at a finite frequency. This picture of a weakly first-order martensitic phase transition has explicitly been proposed by theoretical considerations.^{10,11,13}

Beyond results already expected on the basis of the close relationship between β -Zr and β -Ti, the following additional observations were made.

(1) In pure β -Zr, we found no diffuse elastic intensity ("central peak," "elastic precursor") neither around the ω point nor around the N point. This result is in contradiction to theoretical expectations.^{10,11,13}

(2) Alloying with substitutional or interstitial impurities causes static displacements, giving rise to diffuse elastic scattering located in \mathbf{q} space where low-energy phonons are observed.

ACKNOWLEDGMENTS

Financial support by the German Bundesministerium für Forschung und Technologie, Project Nr. 03-ST1SPH-3 and 03-HE2MUE-0 is gratefully acknowledged.

-
- ¹W. Petry, T. Flottmann, A. Heiming, J. Trampenau, M. Alba, and G. Vogl, *G. Phys. Rev. Lett.* **61**, 722 (1988).
- ²W. Petry, A. Heiming, J. Trampenau, M. Alba, C. Herzig, H. R. Schober, and G. Vogl, *Phys. Rev. B* **43**, 10933 (1991) (referred to hereafter as I).
- ³J. Trampenau, W. Petry, A. Heiming, M. Alba, C. Herzig, and H. R. Schober, *Phys. Rev. B* **43**, 10963 (1991) (referred to hereafter as III).
- ⁴C. Herzig, in *Diffusion in Metals and Alloys*, edited by F. J. Kedves and D. L. Beke (Trans. Tech. Publ., Switzerland, 1983), p. 23.
- ⁵U. Köhler and Chr. Herzig, *Philos. Mag. A* **58**, 769 (1988).
- ⁶W. Petry, A. Heiming, J. Trampenau, and G. Vogl, *Defect and Diffusion Forum*, edited by F. J. Kedves and D. L. Beke (Trans. Tech. Publ. Switzerland, 1989), Vols. 66–69, p. 157.
- ⁷G. Vogl, W. Petry, Th. Flottmann, and A. Heiming, *Phys. Rev. B* **39**, 5025 (1989).
- ⁸S. K. Sikka, Y. K. Vahra, and R. Chidambaram, *Prog. Mater. Sci.* **27**, 245 (1982).
- ⁹Y.-Y. Ye, Y. Chen, K.-M. Ho, B. N. Harmon, and P.-A. Lindgård, *Phys. Rev. Lett.* **58**, 1769 (1987).
- ¹⁰P.-A. Lindgård and O. G. Mouritsen, *Phys. Rev. B* **57**, 2458 (1986).
- ¹¹P. A. Lindgård and O. G. Mouritsen, *Phys. Rev. B* **41**, 688 (1990).
- ¹²V. P. Dmitriev, S. B. Rochal, Yu. M. Gufa, and P. Tolédano, *Phys. Rev. Lett.* **60**, 1958 (1988).
- ¹³J. A. Krumhansl and R. J. Gooding, *Phys. Rev. B* **39**, 3047 (1989).
- ¹⁴F. Willaime and C. Massobrio, *Phys. Rev. Lett.* **63**, 2244 (1989); *Phys. Rev. B* (to be published).
- ¹⁵C. Stassis, J. Zarestky, N. Wakabayashi, *Phys. Rev. Lett.* **41**, 1726 (1978).
- ¹⁶C. Stassis and J. Zarestky, *Solid State Commun.* **52**, 9 (1984).
- ¹⁷Th. Flottmann, W. Petry, R. Serve, and G. Vogl, *Nuclear Instrum. Methods A* **260**, 165 (1987).
- ¹⁸A. Heiming, Ph.D. thesis, Freie Universität Berlin, 1989.
- ¹⁹A. Heiming, W. Petry, J. Trampenau, M. Alba, C. Herzig, and G. Vogl, *Phys. Rev. B* **40**, 11425 (1989).
- ²⁰B. Dörner, *Coherent Inelastic Neutron Scattering in Lattice Dynamics*, Springer Tracts in Modern Physics, Vol. 93 (Springer, Berlin, 1982).
- ²¹S. W. Lovesey, *Theory of Neutron Scattering from Condensed Matter* (Clarendon, Oxford, 1984), Vol. 1, p. 301.
- ²²K.-M. Ho, C.-L. Fu, and B. N. Harmon, *Phys. Rev. B* **28**, 6687 (1983).
- ²³K.-M. Ho, C.-L. Fu, and B. N. Harmon, *Phys. Rev. B* **29**, 1575 (1984).
- ²⁴The broad T_1 [$\xi\xi0$] phonons had been described by a broadened Gaussian shape in Ref. 19. The obtained frequencies are lower and coincide with the channel of the highest count rate.
- ²⁵Y. Chen, C. L. Fu, K.-M. Ho, and B. N. Harmon, *Phys. Rev. B* **31**, 6675 (1985).
- ²⁶See, for instance, S. M. Shapiro, B. X. Yang, G. Shirane, Y. Noda, and L. E. Tanner, *Phys. Rev. Lett.* **62**, 1298 (1989); M. Müller, G. Hergert, M. Keil, G. Eckold, J. B. Suck, W. Weber, and H. Jex, in *The Martensitic Phase Transition in Science and Technology*, edited by E. Horbogen, N. Jost (DGM Informationsgesellschaft Verlag, Germany, 1989), p. 115.
- ²⁷For phase diagrams of gaseous impurities in metals, see *Gas and Kohlenstoff in Metallen*, edited by E. Fromm and E. Gebhard (Springer-Verlag, Berlin, 1976).
- ²⁸J. D. Axe, A. Heidemann, W. S. Howells, S. C. Moss, and R. Pynn, *Solid State Commun.* **24**, 743 (1977).
- ²⁹C. Stassis, J. Zarestky, D. Arch, O. D. McMasters, and B. N. Harmon, *Phys. Rev. B* **18**, 2632 (1978).
- ³⁰J. Zarestky (private communication).
- ³¹R. Hultgren, P. D. Desai, D. T. Hawkins, M. Gleiser, K. K. Kelly, and D. D. Wagman, *Selected Values of the Thermodynamic Properties of the Elements* (American Society for

- Metals, Metals Park, Ohio, 1973).
- ³²B. N. Harmon (private communication).
- ³³C. Zener, *Phys. Rev.* **71**, 846 (1947).
- ³⁴J. Friedel, *J. Phys. (Paris) Lett.* **35**, L59 (1974).
- ³⁵G. Grimvall and I. Ebbsjö, *Phys. Scr.* **12**, 168 (1975).
- ³⁶G. L. Squires, *Proceedings of the Symposium on Inelastic Scattering of Neutrons in Solids and Liquids, Chalk River, 1962* (IAEA, Trieste, 1963), Vol. II, p. 71.